Fast Dynamic Control of PFC Using Boundary Control with a Second-Order Switching Surface

Carl H.M. Ho, Henry S.H. Chung* and Kelvin K.S. Leung

Department of Electronic Engineering
City University of Hong Kong
Tat Chee Avenue, Kowloon Tong
Hong Kong SAR, China
*Tel: (852) 2788 7807
*Fax: (852) 2788 7791
*Email: eeshc@cityu.edu.hk

Abstract - **The difference between the fast dynamics associated with the input current shaping of power factor correctors (PFCs) and the slow dynamics associated with their output voltage regulation is typically exploited by using multiple control loops. The overall dynamic response is generally limited by the output voltage regulation loop. Research into an analogy-based controller for fast dynamic control of PFCs is at a slow pace. This paper applies the concept of the boundary control method with a second-order switching surface for the boost type PFC, so as to achieve fast dynamic response. The method is based on predicting the state trajectory movement after a hypothesized switching action and the output can ideally be reverted to the steady state in two switching actions during the large-signal input voltage and output load disturbances. Theoretical predictions are verified with the experimental results of a 320W, 110V prototype.**

Index Terms – Boundary control, power factor corrector, ac/dc conversion.

I. INTRODUCTION

Nowadays, power factor correction technique is necessary for ac-to-dc power conversion to comply with the requirements of the international standards, such as IEC-1000-3-2 and IEEE-519. Among various possible topologies for the power stage, boost-derived power factor corrector (PFC) is the most popular choice. In the last two decades, many different analog control methods, including average current mode control [1], peak current control [2], hysteresis control [3], sliding-mode control [4], one-cycle control [5], nonlinear carrier control [6], etc, have been proposed. Many integrated circuits for PFCs have also been commercially available. All those methods mainly focus on enhancing the steady-state operation, such as the waveshape of the input current, and/or simplifying the control complexity, such as reducing the number of the sensing variables in the power stage of the PFC. The difference between the fast dynamics associated with the input current shaping and the slow dynamics associated with the output voltage regulation is typically exploited by using multiple control loops [7]. The overall dynamic response is generally limited by the output voltage regulation loop. Research into PFC an analog-based controller for fast dynamic control of PFCs is at a slow pace. By integrating some predictive algorithms, different digital control techniques [8]-[10] for improving the dynamic response of PFC have been proposed. However, the advantages are counteracted by the implementation complexity.

Recently, a new control method using boundary control with a second-order switching surface for fast dynamic control of buck converter has been proposed in [11]. It is based on predicting the state trajectory movement after a hypothesized switching action and the output can ideally be reverted to the steady state in two switching actions during the large-signal input voltage and output load disturbances. By extending the similar concept, a controller for boost-type PFCs is proposed in this paper. Apart from providing a stable dc output and shaping the input current, the PFC can also revert back to the steady state in two switching actions after a large-signal disturbance. A 320W, 110V, prototype has been built. The theoretical prediction and experimental results are in good agreement. Modeling, design, and analysis of the overall system will be given.

II. PRINCIPLE OF OPERATIONS

Fig. 1 shows the boost-type PFC with the proposed controller. Fig. 2 shows the key waveforms of the PFC. The power stage of the PFC can be described by the following state-space equations

$$\dot{x} = A_0\ x + B_0\ v_{in} + (A_1\ x + B_1\ v_S)\ q_1 + (A_2\ x + B_2\ v_S)\ q_2 \tag{1}$$

$$v_o = \begin{bmatrix} 0 & 1 \end{bmatrix} x \tag{2}$$

$$i_S = \begin{bmatrix} 1 & 0 \end{bmatrix} x \tag{3}$$

The work described in this paper was fully supported by a grant from the Research Grants Council of the Hong Kong Special Administrative Region, China (Project No.: CityU 1129/05).

where $x = [i_L \quad v_C]$, A_i and B_i are constant matrices, q_i represents the state of the switch S and D, v_o is the output voltage, and i_S is the input current of the PFC. The elements in A_i and B_i depend on the values of the inductor L, the output capacitor C, and the load R. It can be shown that

$$A_0 = \begin{bmatrix} 0 & 0 \\ 0 & -\frac{1}{RC} \end{bmatrix}, \quad B_0 = \begin{bmatrix} 0 \\ 0 \end{bmatrix},$$

$$A_1 = \begin{bmatrix} 0 & 0 \\ 0 & 0 \end{bmatrix}, \quad B_1 = \begin{bmatrix} \frac{1}{L} \\ 0 \end{bmatrix},$$

$$A_2 = \begin{bmatrix} 0 & -\frac{1}{L} \\ \frac{1}{C} & 0 \end{bmatrix}, \quad B_2 = \begin{bmatrix} \frac{1}{L} \\ 0 \end{bmatrix}.$$

When S is on (off), $q_1 = 1$ (0). When D is on (off), $q_2 = 1$ (0).

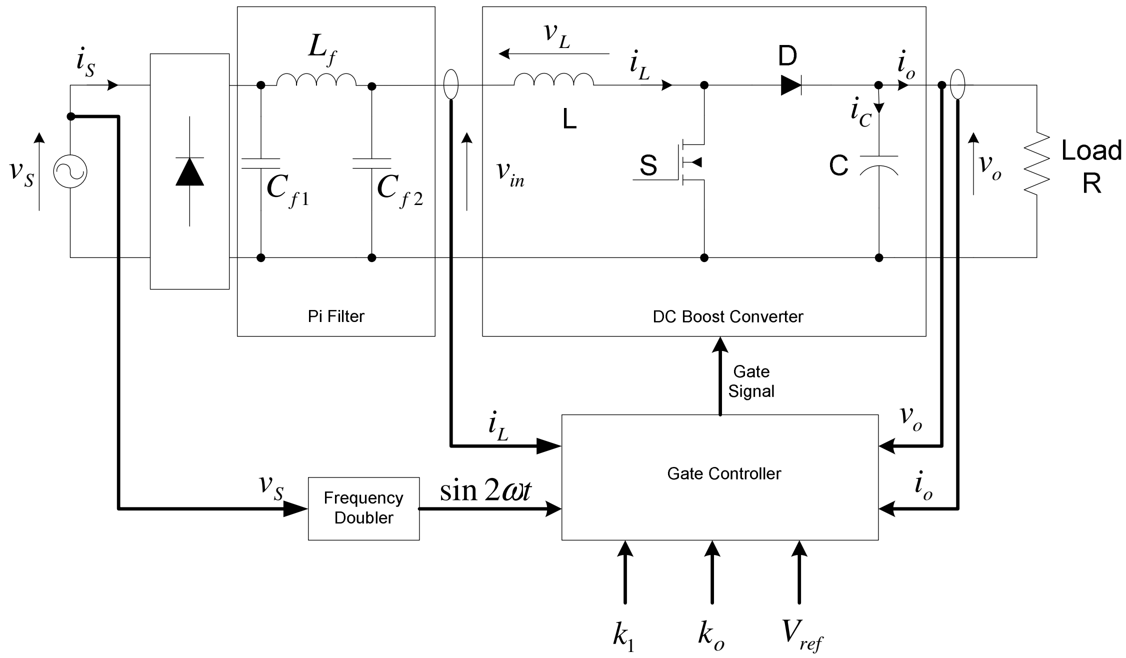

Fig. 1 Boost-type PFC with the proposed controller.

A. Output voltage ripple

v_o consists of a dc component V_{dc} and an ac component Δv_{dc} and is expressed as

$$v_o = V_{dc} + \Delta v_{dc}(t) \tag{4}$$

It gives the output voltage reference $v_{ref}(t)$ that can ensure the input current i_S to be sinusoidal. As shown in [10], $\Delta v_{dc}(t)$ is expressed as

$$\Delta v_{dc}(t) = -k_1 \; I_o \sin 2\omega t \tag{5}$$

where I_o is the output current, $k_1 = 1 / 2\omega C$, C and ω are the output capacitor and angular line frequency, respectively.

B. Derivation of the Switching Surface for a Fixed v_{in}

By solving (1)-(3) with different initial values, Fig. 3 shows a family of state-space trajectories on the two-dimensional plane. The solid lines are named as the *on trajectories* while the dashed lines are named as the *off trajectories*.

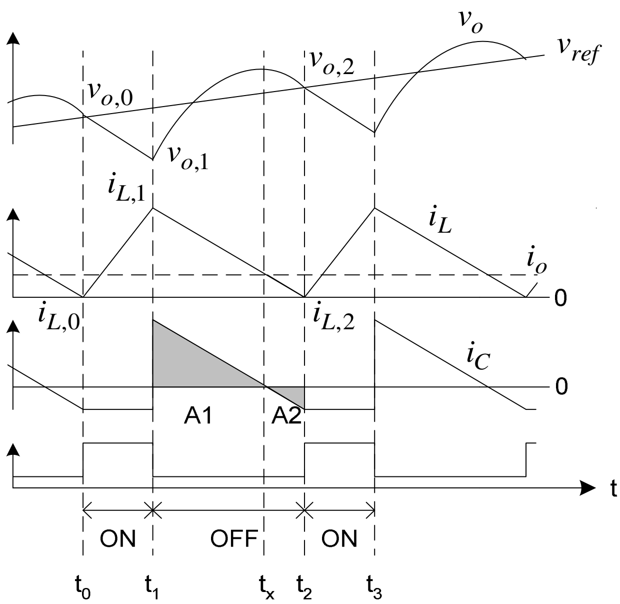

Fig. 2 Key waveforms of the PFC.

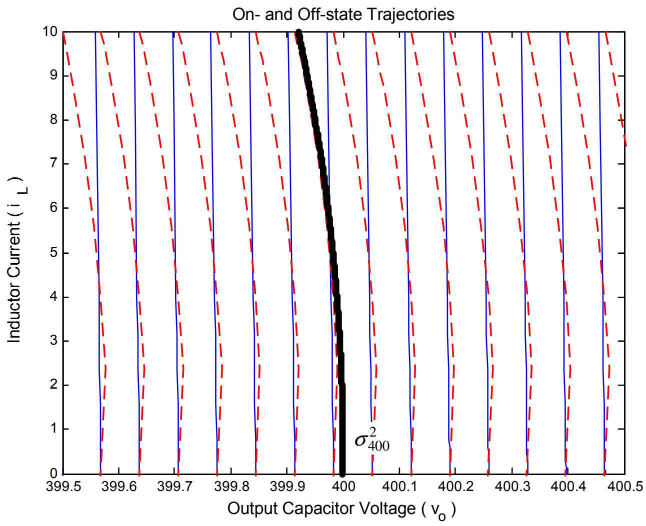

Fig. 3 The state trajectories of the PFC.

As the switching frequency of the switches is much higher than the signal frequency, the load current I_o is relatively constant over a switching cycle and is assumed in the following calculations. This is valid because $\Delta v_{dc}(t)$ << V_{dc}. Thus, the ripple current in i_L is the same as the ripple current in i_C.

As shown in Fig. 2, when S is on and D is off,

$$v_o(t) = -\frac{1}{C_o} I_o\, t + V_{o,0} \tag{6}$$

$$i_L(t) = \frac{1}{L_o} v_{in}\, t + I_{L,0} \tag{7}$$

where $V_{o,0}$ and $I_{L,0}$ are the initial values of v_o and i_L, respectively, at the beginning of this topology, C_o and L_o are the designed values of C and L for the switching surface, respectively.

Thus, by solving (6) and (7), the on-state trajectory { $v_{o,on}$, $i_{L,on}$ } is

$$v_{o,on} = -\frac{L_o}{C_o\, v_{in}} \frac{v_{o,on}}{R} [i_{L,on} - I_{L,0}] + V_{o,0} \tag{8}$$

When S is off and D is on,

$$v_o(t) = \frac{1}{C_o} \int i_c(t)\, dt + V_{o,1} \tag{9}$$

$$i_c(t) = i_L(t) - I_o \tag{10}$$

$$\int i_L(t)\, dt = -\frac{L_o}{2(v_{in} - v_o)} [I_{L,1}{}^2 - i_L{}^2(t)] \tag{11}$$

where $V_{o,1}$ and $I_{L,1}$ are the initial values of v_o and i_L, respectively, at the beginning of this topology.

Thus, by solving (9)-(11), it can be shown that

$$v_o(t) = -\frac{L_o\left(I_{L,1}{}^2 - i_L{}^2(t)\right)}{2C_o\,(v_{in} - v_o)} - \frac{1}{C_o} I_o\, t + V_{o,1} \tag{12}$$

$$i_L(t) = \frac{1}{L_o}(v_{in} - v_o)\, t + I_{L,1} \tag{13}$$

Thus, by solving (12) and (13), the off-state trajectory { $v_{o,off}$, $i_{L,off}$ } is

$$v_{o,off} = \frac{L_o\left(I_{L,1} - i_{L,off}\right)}{2C_o\,(v_{in} - v_o)} \left(\frac{2\, v_{o,off}}{R} - I_{L,1} - i_{L,off} \right) + V_{o,1} \tag{14}$$

When both S and D are off, the trajectory moves along the x-axis and $i_L = 0$.

As discussed in [11], the tangential component of the state-trajectory velocity on the switching surface determines the rate at which successor points approach or recede from the operating point in the boundary control of the switches. An ideal switching surface σ^i that gives fast dynamics should follow the only trajectory passing through the operating point. Although σ^i can ideally go to the steady state in two switching actions during a disturbance, its shape is load-dependent and requires sophisticated computation for solving the only positive and negative trajectories that pass through the operating point.

By the extending the concept in [11] for PFC, the second-order switching surface σ^2 is close to σ^i around the operating point. The concept is based on estimating the state trajectory after a hypothesized switching action. The gate signals to the switches are determined by the following criteria.

1. Turn-on criteria

Consider a generic time instant in a line cycle shown in Fig. 2. v_{in} is assumed to be constant within the switching cycle. As the PFC is operating in critical mode, S is switched on at t_0 when

$$i_L(t_0) \le 0 \quad \text{and} \quad v_o(t_0) \le v_{ref}(t_0)\,. \tag{15}$$

2. Turn-off criteria

During the period of [t_0 , t_1], S is on. i_L increases, according to the equation of

$$\frac{di_L}{dt} = \frac{1}{L_o} v_{in} \tag{16}$$

where L_o is the value of the inductor used in designing the switching surface.

The on time t_{on} (= $t_1 - t_0$) of S is estimated by

$$t_{on} = L_o \frac{i_L(t_1)}{v_{in}(t_1)} \tag{17}$$

The output voltage can be expressed as

$$v_o(t_1) - v_o(t_0) = \frac{1}{C_o}\int_{t_0}^{t_1} i_c(t)dt \tag{18}$$

and can be approximated by using (17) and assume $i_c = -I_o$ in this duration. Thus, (18) becomes

$$v_o(t_0) = \frac{L_o\ I_o}{C_o}\frac{i_L(t_1)}{v_{in}(t_1)} + v_o(t_1) \tag{19}$$

where C_o is the designed value of C in formulating the switching surface.

By using (17) and (19), the slope of v_{ref} at t_1, $\dot{v}_{ref}(t_1)$, is expressed as

$$\dot{v}_{ref}(t_1) \cong \frac{\Delta v_{ref}(t_1)}{\Delta t} = \frac{v_{ref}(t_1) - v_o(t_0)}{t_{on}} = \frac{v_{ref}(t_1) - v_o(t_1) - \dfrac{L_o\ I_o\ i_L(t_1)}{C_o\ v_{in}(t_1)}}{\dfrac{L_o\ i_L(t_1)}{v_{in}(t_1)}} \tag{20}$$

During the period of $[t_1, t_2]$, S is off. The off time t_{off} $(= t_2 - t_1)$ of S is estimated by

$$t_{off} = \frac{L_o\ i_L(t_1)}{v_o(t_1) - v_{in}(t_1)} \tag{21}$$

If v_{ref} varies linearly in one switching cycle,

$$v_{ref}(t_2) \cong v_{ref}(t_1) + \dot{v}_{ref}(t_1)\, t_{off} \tag{22}$$

By putting (20) and (21) into (22), it can be shown that

$$v_{ref}(t_2) = v_{ref}(t_1) + \frac{[v_{ref}(t_1) - v_o(t_1)]\, v_{in}(t_1) - \dfrac{L_o\ I_o\ i_L(t_1)}{C_o}}{v_o(t_1) - v_{in}(t_1)} \tag{23}$$

By assuming that the output capacitor is discharged linearly, the switching time t_x at when $i_C = 0$ is calculated by considering

$$v_o(t_x) - v_o(t_1) = \frac{1}{C_o}\int_{t_1}^{t_x} i_c(t)\, dt \tag{24}$$

$\int_{t_1}^{t_x} i_c(t)dt$ equals the area A1 shown in Fig. 2. If it is approximated by a triangle,

$$\int_{t_1}^{t_x} i_C(t)\, dt \cong \frac{1}{2}\frac{i_c^2(t_1^+)}{di_c/dt} \tag{25}$$

Based on (10),

$$\frac{di_c}{dt} = \frac{di_L}{dt} = \frac{1}{L_o}(v_{in} - v_o) \tag{26}$$

By putting (26) into (25),

$$\int_{t_1}^{t_x} i_c(t)dt = \frac{L_o}{2(v_o - v_{in})} i_c^2(t_1^+) \tag{27}$$

and then putting it into (24),

$$v_o(t_x) - v_o(t_1) = \frac{L_o}{2C_o(v_o - v_{in})} i_c^2(t_1^+) \tag{28}$$

During the period t_x to t_2,

$$v_o(t_2) - v_o(t_x) = -\frac{1}{C_o}\int_{t_x}^{t_2} i_C(t)dt \tag{29}$$

$\int_{t_x}^{t_2} i_c(t)dt$ equals the area of A2 shown in Fig. 2. Again, if it is approximated by a triangle,

$$\int_{t_x}^{t_2} i_c(t)\, dt = \frac{1}{2}\frac{I_o^{\ 2}}{di_c/dt} \tag{30}$$

By using (26),

$$\int_{t_x}^{t_2} i_c(t)dt = \frac{L}{2(v_o - v_{in})} I_o^{\ 2} \tag{31}$$

By putting (31) into (29),

$$v_{ref}(t) - v_o(t_x) = -\frac{L_o}{2\ C_o\ (v_o - v_{in})} I_o^{\ 2} \tag{32}$$

By putting (28) into (32),

$$v_o(t_1) = v_{ref}(t_2) - \frac{k_o}{(v_o - v_{in})}[i_c^2(t_1^+) - I_o^{\ 2}] \tag{33}$$

where $k_o = \dfrac{L_o}{2\ C_o}$.

By putting (23) into (33), eq. (33) gives the criteria of switching S off that

$$v_o(t_1) \ge v_{ref}(t_1) - \frac{k_o}{v_o(t_1)} i_L^{\ 2}(t_1) \quad \text{and} \quad i_L > 0 \tag{34}$$

By combining (15) and (34), the general form of σ^2 is defined as

$$\sigma^2{}_{\Delta+} = \frac{k_o}{v_o} i_L^2 + v_o - v_{ref}, \quad i_L > 0 \tag{35}$$

and

$$\sigma^2{}_{\Delta-} = v_o - v_{ref}, \quad i_L \le 0 \tag{36}$$

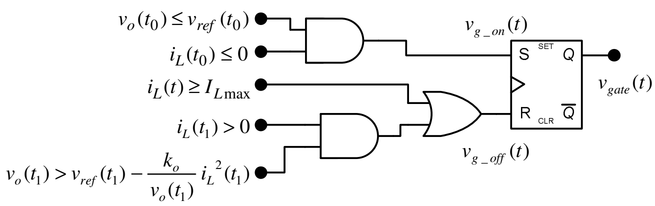

Fig. 4 Implementation of the proposed controller.

S will also be turned off if $i_L > I_{L\max}$, in order to avoid overcurrent of the switch and inductor. Fig. 4 shows the circuit implementation.

III. Steady-State Characteristics

Based on (4) and (5), v_{ref} is expressed as

$$v_{ref}(t) = V_{dc} - k_3\, I_o \sin 2\omega t \tag{37}$$

where $k_3 = \dfrac{1}{2\,\omega\, C_o}$.

Hence, as illustrated in Fig. 2, when the PFC is in discontinuous conduction mode (DCM),

$$v_{o,0} = v_{ref,0}\,,\quad v_{o,2} = v_{ref,2} \tag{38}$$

where $v_o(t_0) = v_{o,0}$, $v_o(t_2) = v_{o,2}$, $i_L(t_0) = i_{L,0}$, and $i_L(t_2) = i_{L,2}$.

The rate of change of v_{ref} is equal to

$$\begin{aligned}\dot{v}_{ref}(t) &= \frac{dv_{ref}}{dt} = -k_3\, I_o \frac{d \sin 2\omega t}{dt} \\ &= -\frac{I_o}{C_o} \cos 2\omega t\end{aligned} \tag{39}$$

Also,

$$v_{ref,1} = v_{ref,0} + \dot{v}_{ref}\, t_{on} \tag{40}$$

Similar to eqs. (6) and (7),

$$v_{o,1} = -\frac{1}{C} I_o\, t_{on} + v_{o,0} \tag{41}$$

$$i_{L,1} = \frac{1}{L} v_{in}\, t_{on} \tag{42}$$

where $v_o(t_1) = v_{o,1}$, and $i_L(t_1) = i_{L,1}$.

By using (40) and (41),

$$\begin{aligned} v_{ref,1} - v_{o,1} &= \left(\dot{v}_{ref} + \frac{1}{C} I_o \right) \frac{L}{v_{in}} i_{L,1} \\ \Rightarrow \quad i_{L,1} &= \left(\frac{v_{ref,1} - v_{o,1}}{L\,\dot{v}_{ref} + 2\,k\,I_o} \right) v_{in} \end{aligned} \tag{43}$$

where $k = \dfrac{L}{2\,C}$.

In DCM, S and D are off from t_2 to t_3. Thus,

$$i_{L,0} = i_{L,2} = 0 \tag{44}$$

By putting (44) into (8),

$$v_{o,1} = -\frac{2\,k}{v_{in}} \frac{v_{o,1}}{R}\, i_{L,1} + v_{o,0} \tag{45}$$

Similarly, by putting (44) into (14),

$$v_{o,2} = \frac{k}{v_{in} - v_{o,2}} i_{L,1} \left(\frac{2 v_{o,2}}{R} - i_{L,1} \right) + v_{o,1} \tag{46}$$

By putting (44) into (35) and (36),

$$\sigma^2{}_{\Delta+} = \frac{k_o}{v_o} i_{L,1}^2 + v_{o,1} - v_{ref,1} = 0 \tag{47}$$

$$\sigma^2{}_{\Delta-} = v_{o,0} - v_{ref,0} = 0 \tag{48}$$

By putting (43) into (47) and (48),

$$\begin{aligned} 0 &= \frac{k_o}{v_{o,1}} \left(\frac{v_{ref,1} - v_{o,1}}{L\,\dot{v}_{ref} + 2\,k\,I_o} \right)^2 v_{in}^2 + v_{o,1} - v_{ref,1} \\ v_{o,1} &= v_{ref,1} - \Psi \end{aligned} \tag{49}$$

where $\Psi = \dfrac{v_{o,1}}{k_o} \left(\dfrac{L\,\dot{v}_{ref} + 2\,k\,I_o}{v_{in}} \right)^2$.

By comparing (47) and (49),

$$i_{L,1} = \frac{v_{o,1}}{k_o} \left(\frac{L\,\dot{v}_{ref} + 2\,k\,I_o}{v_{in}} \right) \tag{50}$$

Let

$$v_{in} = V_m \sin \omega t\,, \quad 0 < \omega t < \pi \tag{51}$$

where V_m is the peak value of the input voltage.

By substituting (39) and (51) into (50),

$$i_{L,1} = \frac{2\,v_{o,1}{}^2}{k_o\, V_m\, R} \left(\frac{k}{\sin \omega t} - \frac{L}{2\,C_o} \frac{\cos 2\omega t}{\sin \omega t} \right) \tag{52}$$

Assume that $v_{o,1} = V_{dc}$, eq. (52) can be expressed as

$$i_{L,1}(t) = \frac{L\, V_{dc}{}^2}{L_o\, V_m\, R} \left[\left(\frac{C_o}{C} - 1 \right) \frac{1}{\sin \omega t} + 2 \sin \omega t \right] \tag{53}$$

It is noted that $i_{L,1}(t)$ is the envelope of the input current. Thus, if $C_o = C$, $i_{L,1}(t)$ and thus the input current are pure sinusoidal. If not, their waveforms will be distorted.

IV. Experimental Verification

A 320W prototype has been built and tested. The component values are: L = 100μH and C = 235μF. v_o is regulated at 400V and the nominal input voltage is 110Vrms, 50Hz. Fig. 5 shows the simulated and experimental steady-state input current and output voltage waveforms with the load resistance of 1kΩ (160W). The experimental results show that the input current is sinusoidal. The measured power factor is 0.996 and the total harmonic distortion of the input current is 6.5%. The experimental results are in close agreement with the simulation results.

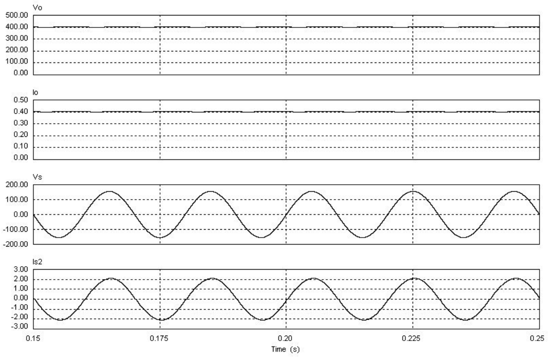

(a) Simulation Results.

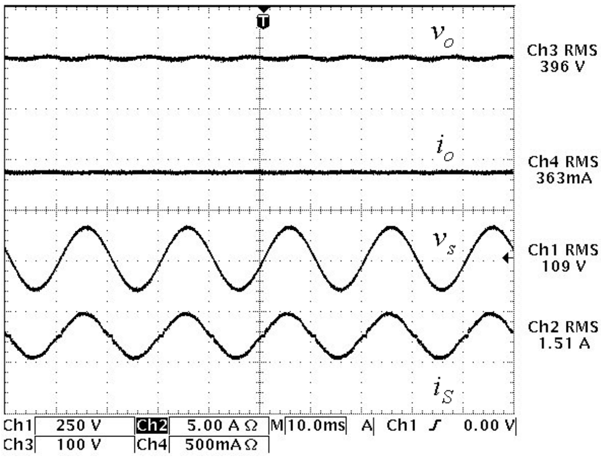

(b) Experimental Results.

Fig.5 Steady State Operation for 160W load. [Ch1:v_s, Ch2:i_s, Ch3:v_o, Ch4:i_o]

Fig. 6 shows the simulated and experimental transient responses of the PFC under a step load change from 1kΩ (160W) to 500Ω (320W). The measured power factor is 0.993 and the total harmonic distortion of the input current is 9%. The input power factor can be maintained at a value higher than 0.97 throughout the operation. Fig. 7 shows the enlarged circuit waveforms. It can be seen that the input current settles into the steady state in two switching actions. Fig. 8(a) shows the input current THD at different voltages and load powers. Fig. 8(b) shows the input power factor at different input voltages and load powers.

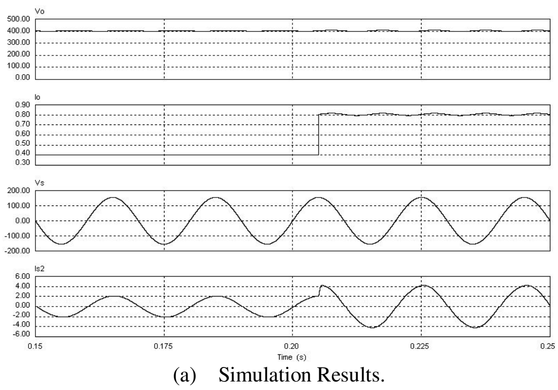

(a) Simulation Results.

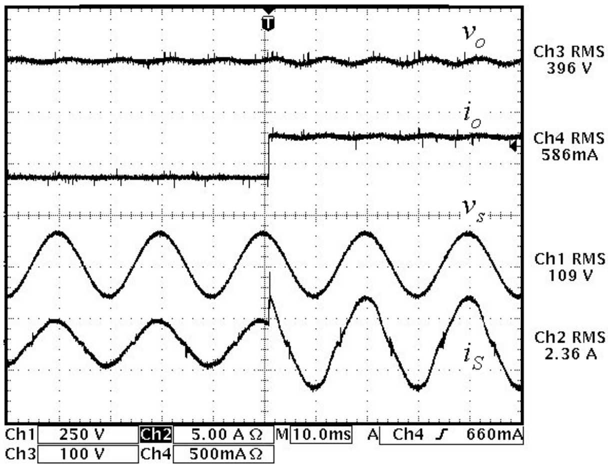

(b) Experimental Results.

Fig.6 Transient responses of the PFC under a step load change from 1kΩ (160W) to 500Ω (320W). [Ch1:v_s, Ch2:i_s, Ch3:v_o, Ch4:i_o]

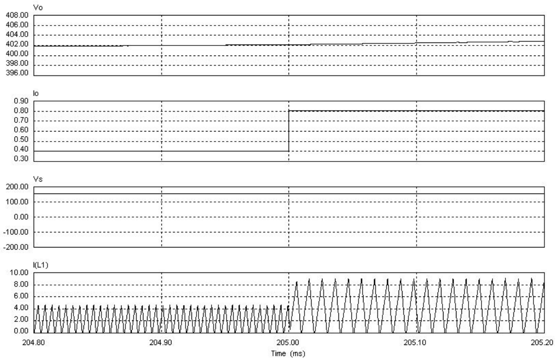

(a) Simulation Result

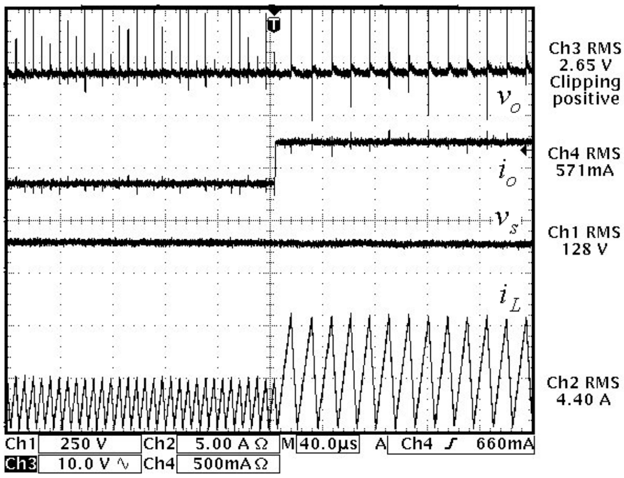

(b) Experimental Results.

Fig.7 Enlarged transient responses shown in Fig. 5. [Ch1:v_s, Ch2:i_L, Ch3:v_o, Ch4:i_o]

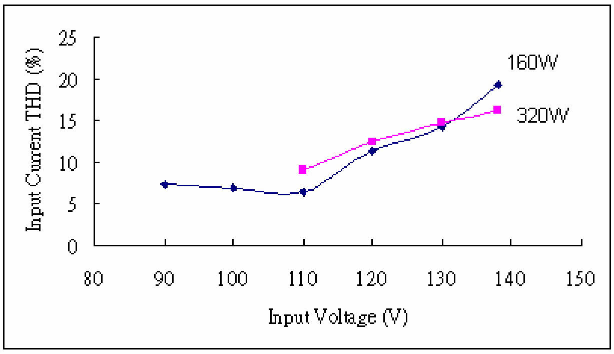

(a) Input current THD.

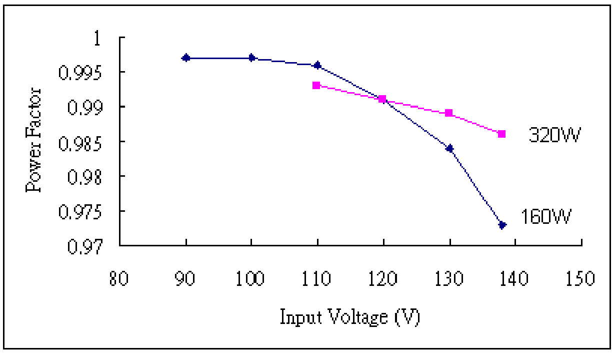

(b) Input power factor.

Fig. 8 Performance characteristics of the PFC at different voltages and load powers.

V. Conclusions

This paper extends the concept of the boundary control method with second-order switching surface for the boost-derived PFC. The converter can give a fast transient response to a large-signal supply and load disturbances. The whole system can revert to steady state within two switching actions when it is subject to large-signal disturbances. The PFC performances have been verified with experimental measurements. Experimental results of a 320W, 110V prototype have been studied.

References

[1] P. C. Todd, "UC3854 controlled power factor correction circuit design," *U-134, Unitrode application Note*, pp. 3-269–3-288.

[2] R. Redl and B. P. Erisman, "Reducing distortion in peak-current-controlled Boost power-factor corretors," in *Proc. IEEE Applied Power Electronics Conf. Expo*, 1994, pp. 576–583.

[3] J. Spangler and A. Behera, "A comparison between hysteretic and fixed frequency Boost converters used for power factor correction," in *Proc. IEEE Applied Power Electronics Conf. Expo*, 1993, pp. 281–286.

[4] L. Rossetto, G. Spiazzi, P. Tenti, B. Fabiano and C. Licitra, "Fast-Response High-Quality Restifier with Sliding Mode Control," *IEEE Trans. Power Electron*., Vol. 9, pp.146 – 152, Mar. 1994.

[5] Z. Lai, K.M. Smedley and Y. Ma, "Time Quantity One-Cycle Control for Power-Factor Correctors," *IEEE Trans. Power Electron*., Vol. 12, pp.369 – 374, Mar. 1997.

[6] R. Zane and D. Maksimovic, "Nonlinear-carrier control for high-power factor rectifiers based on up-down switching converters," *IEEE Trans. Power Electron.*, vol. 13, pp. 213–221, Mar. 1998.

[7] S. Wall and R Jackson, "Fast controller design for single-phase power-factor correction systems," *IEEE Trans. Ind. Electron*., Vol. 44, pp.654 – 660, Oct. 1997.

[8] A. de Castro, P. Zumel, O. Gaecia, T. Riesgo, and J. Uceda, "Concurrent and simple digital controller of an ac/dc converter with power factor correction based on FPGA," *IEEE Trans. Power Electron.*, vol. 18, no. 1, pp. 334-343, Jan 2003.

[9] W. Zhang, G. Feng, Y. Liu and B. Wu, "A digital power factor correction (PFC) control strategy optimized for DSP," *IEEE Trans. Power Electron*., vol. 19, no. 6, pp.1474 – 1485, Nov. 2004.

[10] M. Fu and Q. Chen, "A DSP based controller for power factor correction in a rectifier circuit," in *Proc. 16th Annu. IEEE Applied Power Electronics Conf. Expo*, 2001, pp. 144–149.

[11] K. K. S. Leung and H. Chung, "Derivation of a Second-Order Switching Surface in the Boundary Control of Buck Converters," *IEEE Power Electronics Letter*, vol. 2, no. 2, pp. 63-67, June 2004.